

## Fluxon-density waves in a modulated Josephson ring

A. Shnirman and Z. Hermon

*School of Physics and Astronomy, Raymond and Beverly Sackler Faculty of Exact Sciences,  
Tel-Aviv University, Ramat-Aviv 69978, Israel*

A. V. Ustinov\*

*Institute of Thin Films and Ion Technology, Research Center Jülich, D-52425 Jülich, Germany*

B. A. Malomed†

*Department of Applied Mathematics, School of Mathematical Sciences,  
Raymond and Beverly Sackler Faculty of Exact Sciences, Tel-Aviv University, Ramat-Aviv 69978, Israel*

E. Ben-Jacob

*School of Physics and Astronomy, Raymond and Beverly Sackler Faculty of Exact Sciences,  
Tel-Aviv University, Ramat-Aviv 69978, Israel*

(Received 18 May 1994)

Collective excitations in a fluxon chain placed in a periodically modulated Josephson junction are studied analytically and numerically. In order to eliminate fluxon collisions with boundaries, we consider a Josephson ring (annular Josephson junction). Due to the interaction of the fluxons with periodically placed obstacles, we predict that linear deformation modes of the fluxon chain should bring about resonances which can be observed experimentally. The linear analysis is compared with numerical simulations, and good agreement is found in an appropriate parameter range. In the “relativistic” limit, the numerical simulations reveal a dynamical mode which is characterized by a strongly nonlinear interaction between the moving fluxons in the chain. A qualitative explanation of this regime is suggested by an extrapolation of the linear behavior.

### I. INTRODUCTION

Spatial inhomogeneities in nonlinear media may produce significant effects on dynamics of propagating solitons.<sup>1</sup> When a single soliton interacts with a localized obstacle, it can emit linear waves, get trapped by the obstacle, etc. For a multisoliton lattice placed in the spatially modulated media, one may expect the appearance of linear or nonlinear collective modes.

In a long Josephson junction, solitons are superconducting vortices (magnetic flux quanta or fluxons) described by the perturbed sine-Gordon equation. Since the first theoretical work by Lebowitz and Stephen,<sup>2</sup> collective excitations in a multifluxon chain have received very limited study. The reason probably is that in a typical experiment with homogeneous Josephson junctions it appears to be difficult to excite any collective mode except the progressive motion of a fluxon chain as a whole, known as a flux-flow regime or zero mode. The situation changes if some spatial modulations are present in the system.

Many effects of the single-fluxon interaction with inhomogeneities have been studied theoretically<sup>1,3,4</sup> and some of them also experimentally.<sup>5,6</sup> For the periodic fluxon chain it is natural to consider a periodically modulated medium (e.g., a long Josephson junction with a periodic lattice of inhomogeneities). *Linear* effects, like

coherent emission of linear waves by a chain of equidistant fluxons, produce additional resonance structure on the current-voltage ( $I$ - $V$ ) characteristics of the Josephson junction.<sup>7</sup> *Nonlinear* collective excitations, called super-solitons (i.e., solitary excitations propagating in a pinned fluxon lattice), were found numerically<sup>8</sup> and investigated experimentally<sup>9</sup> and analytically.<sup>10</sup> Such excitations can be viewed as waves of the fluxon density. Another sort of nonlinear fluxon-density excitations was recently found to exist in the fluxon lattice moving in the homogeneous junction with a strong external stimulation at its boundary.<sup>11</sup>

In this paper, we focus on collective excitations in a fluxon chain trapped in a periodically modulated Josephson junction. In order to eliminate collisions with boundaries, we consider a Josephson ring (annular Josephson junction) with a periodic lattice of inhomogeneities (obstacles) shown in Fig. 1. Such a structure has recently been fabricated and studied in experiments.<sup>12</sup> An homogeneous annular junction was studied theoretically in Ref. 13. We predict that linear deformation modes (“phonons”) in the fluxon chain excited by its interaction with the lattice of obstacles should bring about resonances that can be observed experimentally. We compare the linear analysis with numerical simulations, and find good agreement in the appropriate parameter range. In the “relativistic” limit, the numerical simulations reveal a

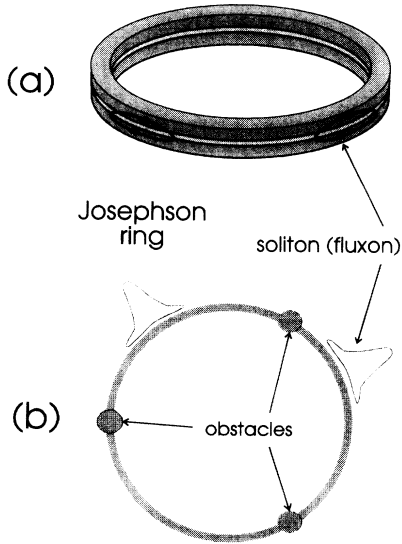


FIG. 1. A sketch of a Josephson ring (a) and its schematic top view (b). The ring contains two trapped fluxons and three equidistantly placed obstacles (inhomogeneities).

dynamic mode which is characterized by a strongly nonlinear interaction between moving fluxons in the chain. On average, we find in this regime one-half of the elementary topological charge (equal  $\pi$  in the sine-Gordon system) effectively moving along the junction. We suggest a qualitative explanation to this regime by an extrapolation of the linear behavior.

## II. LINEAR REGIME

A long Josephson junction is governed by the following equation (known as the perturbed sine-Gordon equation) for the gauge-invariant phase difference across the barrier,  $\Phi$ :

$$\begin{aligned} \Phi_{tt} - \Phi_{xx} + \sin \Phi = J - G\Phi_t \\ + \alpha \sum_{m=1}^N \delta(x - Lm/N) \sin \Phi, \end{aligned} \quad (2.1)$$

where  $J$  is the external current density,  $G$  is the damping coefficient,  $\alpha$  is the amplitude of the obstacles,  $N$  is the number of obstacles, and  $L$  is the length of the junction. Lengths are measured in units of  $\lambda_J$ , the Josephson penetration depth, and time is measured in units of  $\lambda_J/\bar{c}$  ( $\bar{c}$  is the Swihart velocity). We assume the periodic boundary condition

$$\Phi(x + L) = \Phi(x) + 2n\pi, \quad (2.2)$$

which means that there are  $n$  fluxons in the junction.

The left-hand side of Eq. (2.1) is the pure sine-Gordon equation describing the propagation of electromagnetic waves in a dissipationless, unbiased, homogeneous long

Josephson junction. The multifluxon static solution of this equation is

$$\sin \left[ \frac{1}{2} (\Phi_0 - \pi) \right] = \text{sn}(x/k, k). \quad (2.3)$$

The solution is parametrized by  $k$ , the modulus of the elliptic function, which is related to the length of the junction by

$$L = 2nkK(k), \quad (2.4)$$

where  $K(k)$  is the complete elliptic integral of the first kind. Since the sine-Gordon equation is Lorentz invariant, one can obtain a solution describing a moving chain of fluxons by means of the Lorentz transformation from the static solution (2.3):

$$z = \gamma(x - vt), \quad (2.5)$$

$$\tau = \gamma(t - vx), \quad (2.6)$$

where  $\gamma \equiv 1/\sqrt{1 - v^2}$ . Under the action of this transformation the fluxon suffers a Lorentz contraction, but since the length of the junction is fixed in the  $x, t$  frame (the “laboratory frame”), the solution (2.3) is “stretched” by changing the modulus  $k$ . Using the boundary condition (2.2), we get, instead of (2.4), the following relation:

$$\gamma L = 2nkK(k); \quad (2.7)$$

i.e.,  $k$  depends on the velocity  $v$ . We now take into account the first two terms on the right-hand side of Eq. (2.1), which means applying a bias current  $J$  and assuming a finite dissipation  $G$ . The current accelerates the fluxons until the dissipation becomes large enough to maintain an energy balance. The balance condition determines the steady state velocity of the fluxons. This problem was first solved by McLaughlin and Scott<sup>3</sup> for the infinite junction. In the case of an annular junction, the relation between the bias current and the fluxons velocity was obtained by Marcus and Imry:<sup>14</sup>

$$\frac{8\gamma v E(k)}{k} = -\frac{2\pi J}{G}, \quad (2.8)$$

where  $E(k)$  is the complete elliptic integral of the second kind. Eliminating the parameter  $k$  from the system of equations (2.7) and (2.8), one obtains  $v$  as a function of  $J$ . The velocity  $v$  is related to the average voltage  $V$  across the junction, since only moving fluxons induce voltage. For a single fluxon  $v$  is directly proportional to  $V$ . For a general multifluxon solution, where each fluxon is moving with its own velocity, the average voltage is proportional to the sum of the individual velocities (with regard to their signs). Therefore Eq. (2.8) is actually the  $I$ - $V$  characteristic of the junction with  $n$  fluxons. Such characteristics for annular Josephson junctions have been measured experimentally  $n$  varying from 1 to 9.<sup>15</sup>

Let us consider the pure sine-Gordon equation again. Our purpose is to describe the small oscillations about the static multisoliton solution (2.3). This problem was solved by Lebwohl and Stephen<sup>2</sup> for the infinite system. Assuming the solution of the form

$$\Phi = \Phi_0 + \Psi \quad (2.9)$$

and keeping only the terms which are linear in  $\Psi$ , one obtains the following Lamé equation:

$$\Psi_{tt} - \Psi_{xx} + \cos \Phi_0 \Psi = 0. \quad (2.10)$$

Since this equation is linear with a periodic potential, its solutions can be represented in the Bloch (Floquet) form

$$\Psi_0(x, t) = u(x) \exp(iqx) \exp(\pm i\omega_0 t), \quad (2.11)$$

$$u(x + L/n) = u(x),$$

$$u(x) = \frac{H(x/k \pm \beta)}{\Theta(x/k)} \exp\left(\pm i \frac{\pi x}{2kK(k)}\right), \quad (2.12)$$

$$q = \mp \left( \frac{Z(\beta)}{ik} + \frac{\pi}{2kK(k)} \right), \quad (2.13)$$

$$\omega_0^2 = \frac{dn^2(\beta)}{k^2}. \quad (2.14)$$

Here  $H$ ,  $\Theta$ , and  $Z$  are the Jacobi's  $\eta$ ,  $\theta$ , and  $\zeta$  functions, respectively. The signs  $\pm$  imply that for every  $\omega_0$  there are two linearly independent solutions; i.e., all the energy levels are twice degenerated. The solution  $\Psi_0$  is parametrized by a complex parameter  $\beta$  which moves along the contour  $K(k) + iK'(k) \rightarrow K(k) \rightarrow 0 \rightarrow iK'(k)$  on the complex plane as  $\omega_0$  changes from 0 to  $\infty$ . In the intervals  $[K(k) + iK'(k), K(k)]$  and  $[0, iK'(k)]$ , the function  $Z(\beta)$  is purely imaginary and consequently the wave number  $q$  is real. In the interval  $[K(k), 0]$  the function  $Z(\beta)$  is real, and the wave number becomes complex. Therefore, one obtains two zones of small oscillations, which in frequency terms are  $\omega_0 = [0, \frac{1-k^2}{k^2}]$  and  $\omega_0 = [\frac{1}{k^2}, +\infty]$ . Leibold and Stephen interpreted the lower-zone modes as acoustic oscillations of the chain of fluxons, and the higher-zone modes as Josephson plasma oscillations. It is interesting to mention that the width of the gap between these two zones does not depend on  $k$  and is equal to the plasma frequency of the Josephson junction without fluxons. When the density of fluxons tends to zero ( $k \rightarrow 1$ ), the lower zone disappears and only the plasma modes survive.

To apply these results to the annular junction, we should use the periodic boundary condition (2.2). With regard to Eq. (2.9), we obtain the condition

$$\Psi(x + L) = \Psi(x). \quad (2.15)$$

Substituting Eqs. (2.11)–(2.14) and (2.7) (with  $\gamma = 1$ ) into Eq. (2.15), one obtains

$$Z(\beta) = \frac{\pi i(2l - n)}{2nK(k)}, \quad l = 0, \pm 1, \pm 2, \dots \quad (2.16)$$

This is a geometrical quantization condition, which determines the discrete energy levels. Since in the lower

zone the parameter  $\beta$  changes in the interval  $[K(k) + iK'(k), K(k)]$ , and, consequently,  $Z(\beta)/i$  changes in the interval  $[\pi/2K(k), 0]$ , we find that the number of energy levels in this zone is  $[\frac{n}{2}] + 1$ , where  $[\dots]$  stands for the integer part. For  $l = n$ , we obtain  $Z(\beta) = \pi i/2K(k)$ , and  $\omega_0 = 0$ . This is obviously the translational mode. Therefore, we get only  $[\frac{n}{2}]$  nontrivial levels in the lower zone. Recalling the twofold degeneracy, we find that the number of modes is equal to the number of fluxons. (The number of modes in the higher zone is infinite.) In the case of two fluxons in an annular Josephson junction, which will be studied in detail below, only one nontrivial level exists in the lower zone.

Until now we were dealing with small oscillations about static fluxons. To obtain the oscillations about moving fluxons, we Lorentz transform the solution  $\Psi_0$  given by Eqs. (2.11) and (2.12). The periodicity condition (2.15) changes to

$$\Psi(z + \gamma L, \tau + v\gamma L) = \Psi(z, \tau). \quad (2.17)$$

As we have previously seen, this transformation induces a change of the parameter  $k$  according to Eq. (2.7). Since the solution depends now also on  $\tau$ , there is a change in the parameter  $\beta$  as well, which can be obtained by inserting Eqs. (2.11) – (2.14) into Eq. (2.17):

$$Z(\beta) + i\omega_0 v k = \frac{\pi i(2l - n)}{2nK(k)}, \quad l = 0, \pm 1, \pm 2, \dots \quad (2.18)$$

This is the condition which determines the energy levels of the system for the moving fluxon chain.

We are now ready to approach the full problem (2.1). As was said above, under the action of the bias current  $J$  and the dissipation  $G$  the fluxon acquires the steady state velocity  $v$  given by Eq.(2.8). Therefore, every fluxon collides with the obstacles at the frequency

$$\omega = \frac{2\pi N v}{L} \quad (2.19)$$

in the laboratory frame. This means that the obstacles act on the chain of fluxons as a time-periodic force. If the frequency of this force is close to one of the above-mentioned eigenfrequencies  $\omega_0$ , a resonance will occur and the amplitude of this oscillatory mode is expected to be anomalously large. Consequently, this mode will dissipate more energy, and additional current should be applied to compensate for this additional loss. Near the resonance points, nearby all the additional current will be spent to compensate the additional dissipation; thus the velocity of the fluxons, regarded as a function of the current, is expected to be almost constant. Hence one should observe steps in the  $I$ - $V$  characteristic of the junction at the resonance points.

In this section we treat the problem in the linear approximation. This means that we assume the solution to

be of the form (2.9), where  $\Phi_0$  is the moving multifluxon solution with the velocity determined by Eqs. (2.8) and (2.7), and the perturbation  $\Psi$  to be small. Moreover, we assume that  $\alpha$  is small and that  $G$  is large. To check the validity of the linear approximation, we consider evolution of the collective momentum<sup>16</sup>

$$P \equiv - \int \Phi_t \Phi_x = P_0 + p, \tag{2.20}$$

where  $P_0$  stands for the collective momentum of the fluxons, and  $p$  is the momentum of the small oscillations. The equation of motion for  $P$ , which follows directly from Eq. (2.1) is

$$\frac{dP}{dt} = 2\pi nJ - GP - \alpha \sum_{m=1}^N \sin \Phi_0 \left[ \frac{\gamma}{k} \left( \frac{Lm}{N} - vt \right) \right] \Phi_{0x} \left[ \frac{\gamma}{k} \left( \frac{Lm}{N} - vt \right) \right]. \tag{2.21}$$

We have neglected all the terms containing products of  $\alpha$  and  $\Psi$ . The momentum  $P_0$  satisfies Eq. (2.21) with  $\alpha = 0$ , and so we obtain the following equation for  $p$ :

$$\frac{dp}{dt} + Gp = \frac{4\gamma\alpha}{k} \sum_{m=1}^N \operatorname{sn} \left[ \frac{\gamma}{k} \left( \frac{Lm}{N} - vt \right) \right] \operatorname{cn} \left[ \frac{\gamma}{k} \left( \frac{Lm}{N} - vt \right) \right] \operatorname{dn} \left[ \frac{\gamma}{k} \left( \frac{Lm}{N} - vt \right) \right]. \tag{2.22}$$

The right-hand side of this equation is a periodic function of  $t$  and may be represented by its Fourier expansion. For our purposes, we will keep the first harmonic only. Thus Eq. (2.22) becomes

$$\frac{dp}{dt} + Gp = \frac{4\gamma\alpha c}{k} \exp(i\Omega t), \tag{2.23}$$

where  $\Omega \equiv \frac{2\pi Nnv}{L}$  is the fundamental frequency, and  $c$  is some constant of the order of one. Without the force exerted by the obstacles, the solution for  $p$  is a decaying one. The amplitude of the steady state solution of Eq. (2.23) is

$$A = \frac{4\gamma\alpha c}{k\sqrt{G^2 + \Omega^2}}. \tag{2.24}$$

The linear approximation demands that the ratio  $\frac{A}{P_0}$  must be much smaller than 1. This yields

$$\frac{\alpha}{4vE(k)\sqrt{G^2 + \frac{4\pi^2 N^2 n^2 v^2}{L^2}}} \ll 1. \tag{2.25}$$

A simple analysis of the left-hand side of this inequality shows that, in both limits  $v \rightarrow 0$  and  $v \rightarrow 1$ , it diverges, and consequently the linear approximation does not hold. But for intermediate values of  $v$  this ratio can be small if  $\frac{\alpha}{Gv} \ll 1$ . Thus our assumptions are self-consistent.

We now consider the linearized equation for the phase perturbation  $\Psi$  following from Eqs. (2.1) and (2.9):

$$\begin{aligned} \Psi_{tt} - \Psi_{xx} + \cos \Phi_0 \Psi + G\Psi_t \\ = \alpha \sum_{m=1}^N \delta \left( x - \frac{Lm}{N} \right) \sin \Phi_0. \end{aligned} \tag{2.26}$$

The equation is now written in the laboratory frame and the multifluxon solution  $\Phi_0$  is supposed to be moving. It would be natural to transform this equation in order to obtain a static potential. But, using the full Lorentz transformation, one gets a very inconvenient boundary condition (2.17). The most suitable choice of coordinates

for this system is the moving spatial coordinate  $z$  and the laboratory time  $t$ . In these variables Eq. (2.26) is

$$\begin{aligned} \Psi_{tt} - \Psi_{zz} - 2\gamma v \Psi_{zt} + \cos \Phi_0(z) + G\Psi_t - G\gamma v \Psi_z \\ = \alpha \sum_{m=1}^N \delta \left( \frac{z}{\gamma} + vt - \frac{Lm}{N} \right) \sin \Phi_0(z). \end{aligned} \tag{2.27}$$

The boundary condition becomes

$$\Psi(z + \gamma L, t) = \Psi(z, t). \tag{2.28}$$

The right-hand side of Eq. (2.27) is a periodic function of time, and so we can expand it into the Fourier series. In this work, we keep only two first terms of this expansion. For the  $\delta$ -like obstacles, this seems problematic, since in this case all the coefficients of the expansion are equal. But in realistic junctions obstacles should be described by smoothed functions of a finite width, and so the coefficients in front of the higher harmonics of the Fourier expansion are expected to decay. Moreover, if the fluxon density is not very large, namely, if  $k$  is not much smaller than 1, the width of the gap is much larger than the width of the lower zone. In the case of two fluxons in the ring, we have only one nontrivial level in the lower zone, so that the next few harmonics belong to the gap and are unexcitable. Low fluxon density can be achieved either by trapping just a few fluxons in the junction, or by working with a very long junction. In the linear approximation, we therefore obtain the following expression for the right-hand side of Eq. (2.27):

$$\alpha \sin \Phi_0(z) \frac{N^2}{L} \left\{ 1 + 2 \cos \left[ \frac{2\pi N}{L} \left( \frac{z}{\gamma} + vt \right) \right] \right\}. \tag{2.29}$$

We see that the perturbing force is proportional to  $\frac{\alpha N^2}{L}$ , and so this parameter must be small in order that the linear approximation will be valid. This means that the number of obstacles must not be large (in our numerical calculations we consider the case of  $N = 3$ ). Since the left-hand side of Eq. (2.27) is linear, we look for a solu-

tion of the form  $\Psi_1(z) + \Psi_2(z, t)$ , where  $\Psi_1$  is produced by the constant part of the expression (2.29), and  $\Psi_2$  is the oscillating solution produced by the second term of Eq. (2.29).  $\Psi_1$  is a solution of the ordinary differential equation with periodic boundary conditions. It is uniquely determined, and can be interpreted as a small static perturbation of the multifluxon solution,  $\Phi_0$ , caused by the obstacles. We do not find  $\Psi_1$  explicitly. Finding the solution  $\Psi_2$  is much more interesting since it can resonate with the perturbing force. First of all, we determine the velocity of fluxons for which the resonance occurs. It is given by equating the perturbing frequency and the eigenfrequency of the mode  $\Psi_0$ . Let us write the expression for  $\Phi_0$  in terms of the variables  $z$  and  $t$ :

$$\Psi_0 = u(z) \exp(iq'z) \exp\left(\pm i \frac{\omega_0}{\gamma} t\right), \quad (2.30)$$

$$q' \equiv \mp \left( \frac{Z(\beta)}{ik} + \omega_0 v + \frac{\pi}{2K(k)k} \right). \quad (2.31)$$

We see that the frequency in these variables is  $\frac{\omega_0}{\gamma}$ , and so the resonance condition is

$$A \frac{d^2 a}{dt^2} + \left( i \frac{2A\omega_0}{\gamma} - 2iB\gamma v + AG \right) \frac{da}{dt} - i \left( \frac{A\omega_0 G}{\gamma} + BG\gamma v \right) a = C \exp \left[ i \left( \omega - \frac{\omega_0}{\gamma} \right) t \right]. \quad (2.35)$$

The coefficients  $A$ ,  $B$ , and  $C$  stand for the following integrals:

$$A \equiv \int_0^{\gamma L} \Psi_0 \Psi_0^* dz, \quad (2.36)$$

$$B \equiv -i \int_0^{\gamma L} \Psi_{0z} \Psi_0^* dz, \quad (2.37)$$

$$C \equiv \frac{2N^2 \alpha}{L} \int_0^{\gamma L} \sin \Phi_0 \exp \left( \frac{2\pi i N z}{\gamma L} \right) \Psi_0^* dz. \quad (2.38)$$

Looking for  $a(t)$  in the form  $a(t) = b \exp[i(\omega - \frac{\omega_0}{\gamma})t]$ , we finally obtain

$$b = C \left[ -A \left( \omega - \frac{\omega_0}{\gamma} \right)^2 - 2A \frac{\omega_0}{\gamma} \left( \omega - \frac{\omega_0}{\gamma} \right) + 2B\gamma v \left( \omega - \frac{\omega_0}{\gamma} \right) + iAG \left( \omega - \frac{\omega_0}{\gamma} \right) - iAG \frac{\omega_0}{\gamma} - iBG\gamma v \right]^{-1}. \quad (2.39)$$

At the resonance point,  $b$  becomes

$$b_{\text{res}} = i \frac{C}{AG \frac{\omega_0}{\gamma} + BG\gamma v}. \quad (2.40)$$

Since the integrals  $A$  and  $B$  are both real, we see that there is a phase shift of  $\pi/2$  between the oscillatory mode and the perturbing force. This is the well-known property of an oscillator driven by an external resonant force. This means that when the driving force is minimal, the displacement of the oscillator is maximal, and vice versa. In our system, the force is maximal when one of the fluxons is exactly at the position of the obstacle. So, when the perturbation of the phase is maximal, one of the obstacles is exactly in the middle between two fluxons (here we consider the case  $n = 2$ ).

$$\frac{\omega_0}{\gamma} = \omega. \quad (2.32)$$

With regard to Eqs. (2.14) and (2.19), this leads to the equation

$$\frac{dn(\beta)}{\gamma k} = \frac{2\pi v N}{L}. \quad (2.33)$$

This equation, together with Eqs. (2.7) and (2.18), constitutes a system of three equations for the three unknown quantities  $v$ ,  $k$ , and  $\beta$ . Solving this system, one can find their values at the resonance point.

We now look for the amplitude and phase of the oscillation mode at the resonance point. We suppose that in a vicinity of this point the spatial form of  $\Psi_2$  differs only slightly from the form of  $\Psi_0$ . Thus we can project the equation of motion onto the function  $\Psi_0(z, t)$ . We assume that

$$\Psi_2(z, t) = a(t) \Psi_0(z, t), \quad (2.34)$$

and substitute Eq. (2.34) into Eq. (2.27). Next, we multiply the resultant by  $\Psi_0^*$ , and integrate it in  $z$  over the complete period to obtain

Finally, we can find the height of the step in the  $I$ - $V$  characteristic corresponding to this resonance, i.e., the additional amount of current needed to compensate the dissipation caused by the resonantly excited acoustic mode. Starting with the energy balance equation used by McLaughlin and Scott,<sup>3</sup>

$$\frac{dE}{dt} = \int_0^L (-G\Phi_t^2 + J\Phi_t) dx, \quad (2.41)$$

we expand  $\Phi$  as in Eq. (2.9), and we look for the full current  $J$  as  $J = J_0 + \Delta J$ , where  $J_0$  is the current corresponding to the resonant value of the velocity in the homogeneous system according to Eq. (2.8). The linear order vanishes, and at second order we obtain the following expression for  $\Delta J$ :

$$\begin{aligned} \Delta J &= -\frac{G}{2n\pi v\gamma} \int_0^{\gamma L} dz (\Psi_t - \gamma v \Psi_z)^2 \\ &= -\frac{G|b_{\text{res}}|^2}{4n\pi v\gamma} \left( \frac{\omega_0^2}{\gamma^2} A - \gamma v D \right), \end{aligned} \quad (2.42)$$

where  $A$  is defined by (2.36), and

$$D \equiv \int_0^{\gamma L} \Psi_{0z} \Psi_{0z}^* dz. \quad (2.43)$$

### III. NUMERICAL SIMULATIONS

In order to verify the theoretical predictions of the previous section, the  $I$ - $V$  characteristics for various values of the Josephson-junction length  $L$  were obtained by direct numerical simulations of the model (2.1) with the periodic boundary conditions (2.2). As was mentioned in Sec. II, the  $I$ - $V$  characteristic is given by the dependence of the average fluxon velocity  $v$  on the applied external current density  $J$ . Due to the small dissipation, a typical  $I$ - $V$  characteristic displays several hysteretic branches (steps); i.e., for a single value of  $J$  several stable states with different  $v$  exist. The actual state of the system depends on the history of the bias current  $J$ .

While varying  $L$  in the range from 3 to 12, we focused on the case of  $N = 3$  inhomogeneities (i.e., of 3 periods of spatial modulation inside the ring) with two trapped fluxons ( $n = 2$ ). This particular case is illustrated by Fig. 1. In the simulations the coefficient  $g(x) \equiv 1 - \alpha \sum_{m=1}^N \delta(x - Lm/N)$  [see Eq. (2.1)] was approximated by a smooth hyperbolic function<sup>17</sup> as shown in the inset of Fig. 2. The spatial discretization step in the simulations was  $\Delta x = 0.025$ . Each  $I$ - $V$  characteristic was calculated first up (increasing  $J$ ) and then down (decreasing  $J$ ). In every point of the  $I$ - $V$  curve, the integration was performed until a stationary dynamic state was attained. After that, the bias current density  $J$  was increased (or decreased, depending on the actual branch of the hysteretic  $I$ - $V$  curve), and the numerical integration was continued using the final conditions of the previous point. In the  $I$ - $V$  characteristics shown below instead of the averaged voltage  $V$  we plot the average velocity  $v = V/n$  per fluxon. The typical relative accuracy of the dc voltage averaging was  $10^{-4}$ .

An example of the complete  $I$ - $V$  curve is shown in Fig. 2. The parameters are  $L = 5$ ,  $G = 0.02$ ,  $\alpha = 0.2$ , i.e., weak damping and rather strong modulation. This characteristic displays three very pronounced resonances at  $v$  just below 1.0, 0.5, and at about 0.25. The dynamic states corresponding to these three regimes are illustrated by Fig. 3, showing the evolution of the spatial derivative of the phase difference  $\Phi_x(x, t)$ . Physically,  $\Phi_x$  corresponds to a local magnetic field which has a maximum in the center of each fluxon. In Fig. 3 the field  $\Phi_x$  is shown as a function of  $x$  and  $t$  in a grey scale, with white parts corresponding to the highest values of the field. Thus, two white domains in Fig. 3(a) moving from right to left with increasing  $t$  correspond to two fluxons moving with

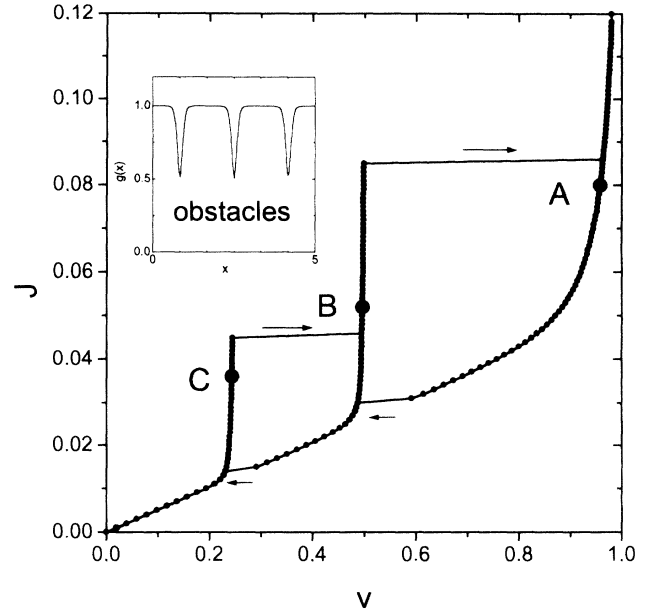


FIG. 2. The numerically calculated  $I$ - $V$  curve for the Josephson ring shown in Fig. 1 with the parameters  $L = 5$ ,  $G = 0.02$ ,  $\alpha = 0.2$ . Under the influence of the bias current density  $J$ , the fluxons move with an average velocity  $v$ . At the top (bottom) of each resonant step, the system switches to a different branch, as indicated by the arrows. The inset shows the spatial modulation produced by the obstacles.

velocity close to the maximal velocity ( $v = 1$ ). In contrast, the state shown in Fig. 3(b) indicates a solitary excitation moving in the opposite direction. This regime coincides with the so-called supersoliton mode.<sup>8,10</sup> In this mode, one may regard the two-fluxon state as a superposition of three static fluxons pinned by the three obstacles and a single antifluxon associated with the darkest area in Fig. 3(b) moving to the right.

The most essential regime for the present work is the third one shown in Fig. 3(c). It looks somewhat surprising by its clear indication of a well-localized single light domain moving with almost the maximal velocity to the left. If one assumes that this domain is the only localized kink which contributes to the dc voltage, this must be a  $\pi$  kink, and not the usual  $2\pi$  kink of the sine-Gordon system (note that the voltage at this point is 0.5). We will address this issue in more detail in the next section.

Figure 4 presents the most interesting parts of the  $I$ - $V$  characteristics calculated for the stronger damped case ( $G = 0.1$ ), using different lengths  $L$  of the ring and  $\alpha = 0.1$ . In Fig. 5 we show a comparison of the theoretical prediction of the previous section with the numerical data for the resonance region positions (shown by arrows in Fig. 4). Since the system of Eqs. (2.7), (2.33), and (2.18) is very complicated, we solved it numerically. From this solution we get the velocity at the resonance point as a function of the junction's length,  $v = v(L)$ , which is, actually, the position of the step on the  $I$ - $V$  characteristic. We see that the function  $v(L)$  (the solid line in Fig. 5) has a maximum at about  $L = 5.5$ . Comparing the theoretical and numerical values of the

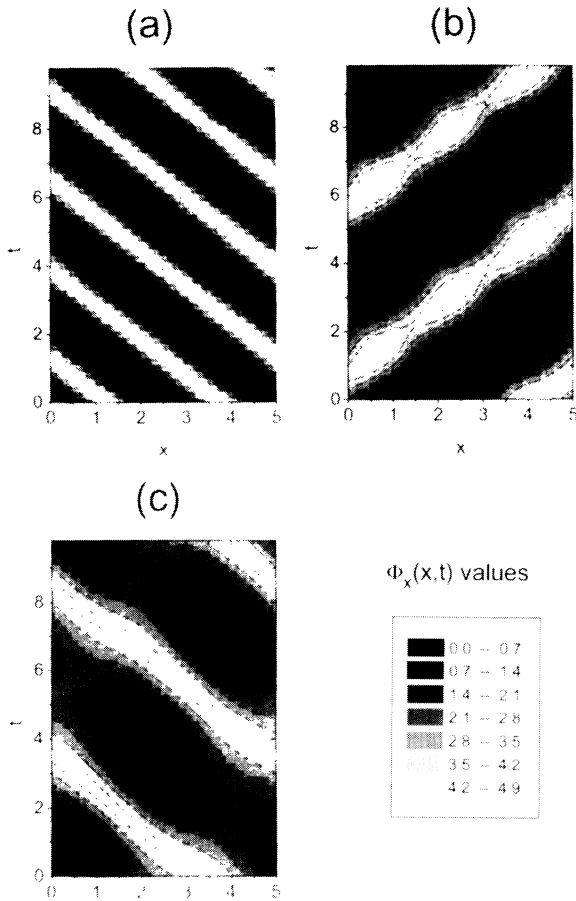


FIG. 3. The spatiotemporal evolution of  $\Phi_x(x,t)$  corresponding to the different points of the  $I$ - $V$  characteristic shown in Fig. 2: (a) the point A, (b) the point B, (c) the point C.

voltage, we see a good accord for  $L > 5$ , i.e., for the region where the analytical method produces  $v$  to be a decreasing function of  $L$ . For  $L < 5$ , the direct simulations show that  $v$  tends to saturate to the value 0.25 as  $L$  goes to zero. The failure of the analytical method in this region is not surprising, since the linear approximation is valid for sufficiently long junctions only, as we have shown above. We will discuss this case in the next section, considering a strongly nonlinear behavior.

#### IV. NONLINEAR REGIME

When the parameter  $\frac{\alpha}{Gv}$  becomes large, or the length of the junction is small, the linear approximation fails. Typical numerical results for this range are shown in Fig. 6. This figure presents fragments of the  $I$ - $V$  characteristic in the underdamped regime ( $G = 0.02$ ), calculated for different lengths of the ring and for a rather strong modulation strength  $\alpha = 0.2$ . The resonance velocity  $v$  proves to be an almost constant function of  $L$  with values close to 0.25. Furthermore, for large rings ( $L = 7.5$  and

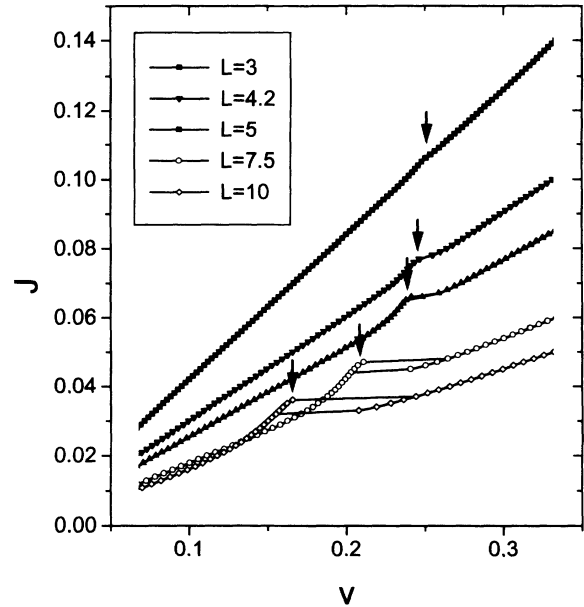


FIG. 4. The  $I$ - $V$  characteristics in the moderately damped regime ( $G = 0.1$ ), calculated for different lengths  $L$  of the Josephson junction. The arrows show positions of the resonance related to the excitations of the fluxon-density waves. The modulation amplitude is  $\alpha = 0.1$ .

10) the resonance splits in two: The lower one is very close to the prediction of the linear analysis (see Fig. 5), and the higher resonance remains close to the “golden value” of 0.25. In order to discriminate between these two regimes (the points  $D$  and  $E$  in Fig. 6), we display in Fig. 7 two-dimensional graphs of the magnetic field  $\Phi_x$  as a function of  $x$  and  $t$ . Both pictures show one localized region of high density moving to the left with the maximal (Swihart) velocity. One can also detect a

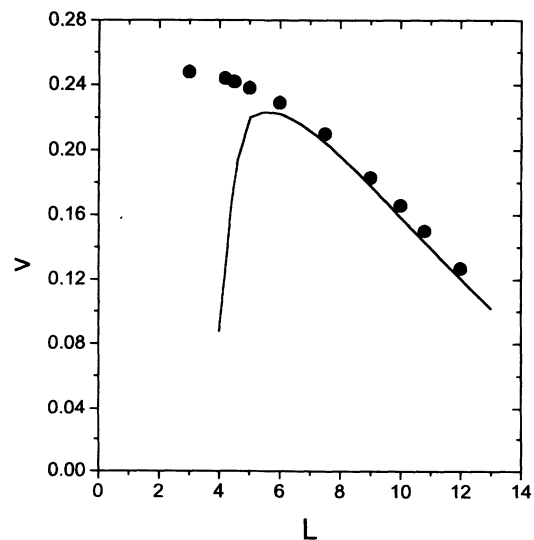


FIG. 5. Comparison of the numerical data (the points) with the analytical result (the continuous line) obtained from Eqs. (2.7), (2.33), and (2.18).

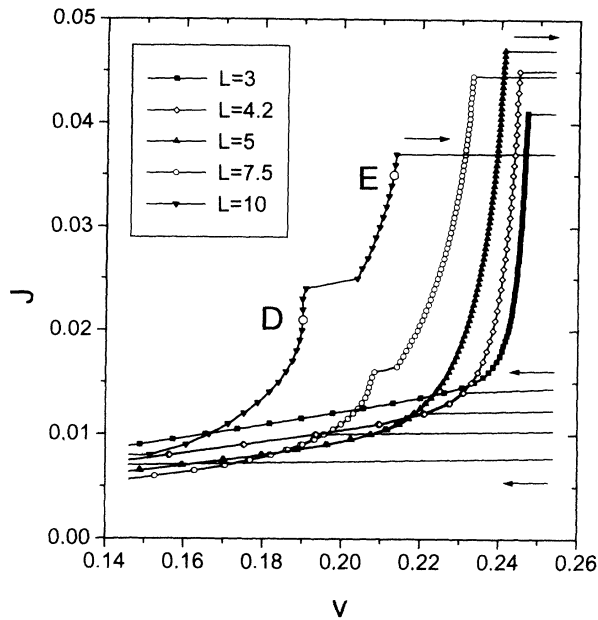


FIG. 6. Fragments of the  $I$ - $V$  characteristics in the underdamped regime ( $G = 0.02$ ), calculated for different lengths  $L$  of the ring. The arrows show the switching directions. The modulation amplitude is  $\alpha = 0.2$ .

second region of high density, somewhat less localized, moving to the right with about half of the Swihart velocity. We interpret these two regions as two fluxons, colliding periodically. Calculating the average voltage produced by these fluxons, we obtain  $V \approx 1 - 0.5 = 0.5$ ; thus  $v = V/n \approx 0.25$ , which is the golden value shown in the  $I$ - $V$  characteristics. In contrast to the rather smooth oscillations of the fluxon position in Fig. 7(a), Fig. 7(b) indicates a strongly relativistic dynamics with hard collisions of the well-localized fluxons.

Qualitatively, we explain the nonlinear regime by an extrapolation of the linear behavior. As was mentioned in Sec. II, there is a phase shift of  $\pi/2$  between the vibration of the fluxons and the driving force produced by the obstacles. Thus, when the two fluxons are closest to each other, one obstacle is located just between them. In the nonlinear regime, where the amplitude of the vibration becomes large, the fluxons will eventually collide, and due to the phase shift the collision will take place exactly at the location of one of the obstacles. The next collision should also occur at an obstacle. Since we have two fluxons and three obstacles (placed at  $x = 1.67, 5.0,$  and  $8.33$  in Fig. 7), this can only happen if one of the fluxons will reach the nearest obstacle, which is at the distance  $\frac{L}{3}$  away, exactly when the other fluxon will reach the same obstacle moving in the opposite direction, thus covering a distance twice as large,  $\frac{2L}{3}$ . Since in the strongly nonlinear regime the velocity of any fluxon is limited by the Swihart velocity, we conclude that the fast fluxon moves with almost the Swihart velocity, while the slower one has to have, on average, half of this velocity. The velocities are exchanged after each collision [see Fig. 7(b)], just

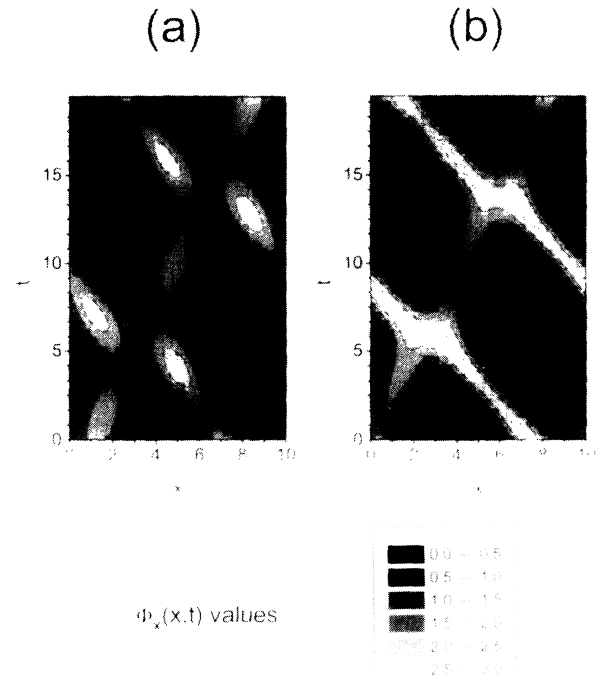


FIG. 7. The spatiotemporal evolution of  $\Phi_x(x,t)$  corresponding to the different points of the  $I$ - $V$  characteristics shown in Fig. 6: (a) the point  $D$ , (b) the point  $E$ .

as with two identical massive particles.

Instead of this picture of two fluxons going back and forth between the collisions, one may think of two fluxons moving through each other without changing their velocities (this qualitative picture is somewhat less physical, as two fluxons repel each other). Since the ideal fluxons are solitonic solutions of the completely integrable sine-Gordon equation, the collisions are totally elastic, their sole effect being spatial shifts, which can be positive or negative. In our case the velocities of the colliding fluxons are opposite; therefore both spatial shifts are positive. These spatial shifts produce a contribution to the mean velocities, which renders them larger than the real velocities (the velocities between collisions). We have seen this effect in the two-dimensional plots. Recall that the mean velocity of the fast fluxon seems to be the Swihart velocity. We are not sure if this velocity is simply close to its limit value, or there is some mechanism enforcing it to be exactly equal to the Swihart velocity.

#### ACKNOWLEDGMENTS

This research was partially supported by a grant from the Israeli Ministry of Energy and a grant from the Wolfson Foundation via the Israeli Academy of Sciences. One of us (Z.H.) thanks the Ministry of Sciences for financial support.

- \* Electronic address: a.ustinov@kfa-juelich.de  
† Electronic address: malomed@leo.math.tau.ac.il
- <sup>1</sup> Yu. S. Kivshar and B. A. Malomed, *Rev. Mod. Phys.* **61**, 763 (1989).  
<sup>2</sup> P. Lebowitz and M. J. Stephen, *Phys. Rev.* **163**, 376 (1967).  
<sup>3</sup> D. W. McLaughlin and A. C. Scott, *Phys. Rev. A* **18**, 1652 (1978).  
<sup>4</sup> Yu. S. Gal'pern and A. T. Filippov, *Solid State Commun.* **48**, 665 (1983); *Sov. Phys. JETP* **86**, 1527 (1984).  
<sup>5</sup> M. Cirillo, *J. Appl. Phys.* **58**, 3217 (1985).  
<sup>6</sup> A. N. Vystavkin, Yu. F. Drachevsky, V. P. Koshelets, and I. L. Serpuchenko, *Fiz. Nizk. Temp.* **14**, 646 (1988) [*Sov. J. Low Temp. Phys.* **14**, 324 (1988)].  
<sup>7</sup> B. A. Malomed and A. V. Ustinov, *Phys. Rev. B* **41**, 254 (1990).  
<sup>8</sup> A. V. Ustinov, *Phys. Lett. A* **136**, 155 (1989).  
<sup>9</sup> V. A. Oboznov and A. V. Ustinov, *Phys. Lett. A* **139**, 481 (1989).  
<sup>10</sup> B. A. Malomed, *Phys. Rev. B* **41**, 2616 (1990).  
<sup>11</sup> O. H. Olsen, A. V. Ustinov, and N. F. Pedersen, *Phys. Rev. B* **48**, 13133 (1993).  
<sup>12</sup> I. V. Vernik, V. A. Oboznov, and A. V. Ustinov, *Phys. Lett. A*, **168**, 319 (1992).  
<sup>13</sup> Z. Hermon, A. Stern, and E. Ben-Jacob, *Phys. Rev. B* **49**, 9757 (1994).  
<sup>14</sup> P. M. Marcus and Y. Imry, *Solid State Commun.* **33**, 345 (1980).  
<sup>15</sup> A. V. Ustinov, T. Doderer, R. P. Huebener, N. F. Pedersen, B. Mayer, and V. A. Oboznov, *Phys. Rev. Lett.* **69**, 1815 (1992).  
<sup>16</sup> D. J. Bergman, E. Ben-Jacob, Y. Imry, and K. Maki, *Phys. Rev. A* **27**, 3345 (1983).  
<sup>17</sup> A. A. Golubov and A. V. Ustinov, *IEEE Trans. Magn.* **MAG-23**, 781 (1987).

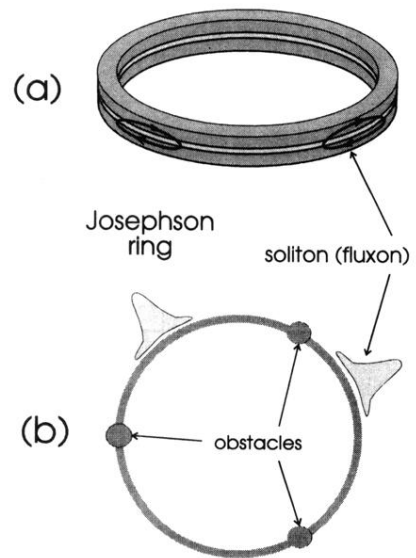


FIG. 1. A sketch of a Josephson ring (a) and its schematic top view (b). The ring contains two trapped fluxons and three equidistantly placed obstacles (inhomogeneities).

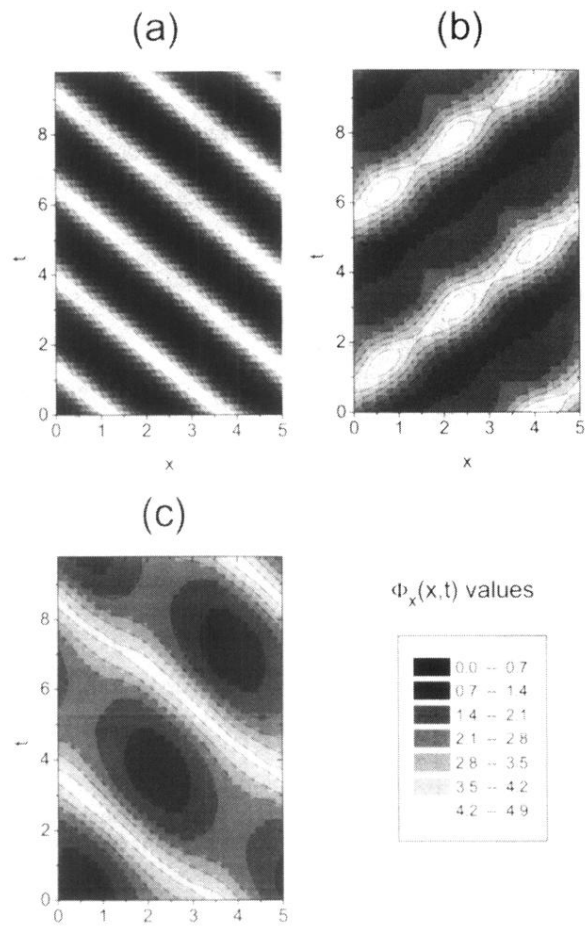


FIG. 3. The spatiotemporal evolution of  $\Phi_x(x,t)$  corresponding to the different points of the  $I$ - $V$  characteristic shown in Fig. 2: (a) the point  $A$ , (b) the point  $B$ , (c) the point  $C$ .

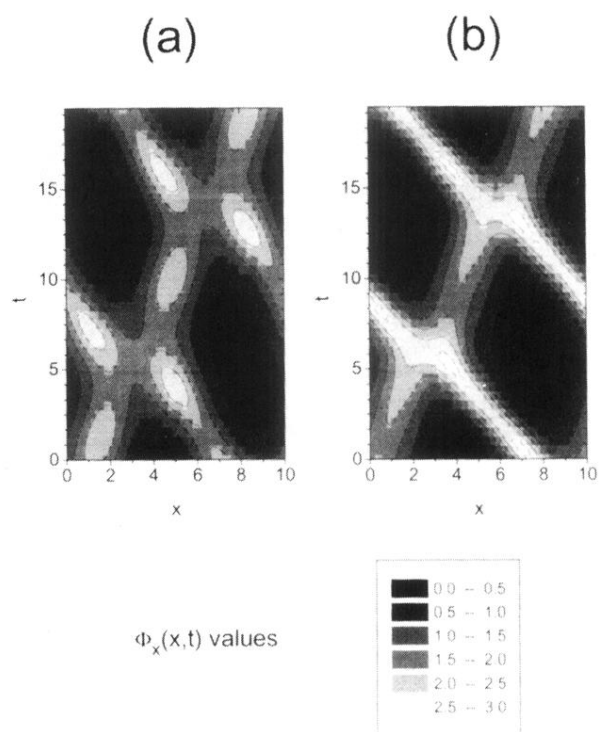


FIG. 7. The spatiotemporal evolution of  $\Phi_x(x,t)$  corresponding to the different points of the  $I$ - $V$  characteristics shown in Fig. 6: (a) the point  $D$ , (b) the point  $E$ .